# Analysis of Performance of the Optimized Divertor in ITER

A.S. Kukushkin[1], H.D. Pacher[2], A. Loarte[1], V. Komarov[1], V. Kotov[3],
M. Merola[1], G.W. Pacher[4], D. Reiter[3]

[1]ITER Organization, Cadarache, France; [2]INRS-EMT, Varennes, Québec, Canada;
[3]FZ Jülich, Jülich, Germany; [4]Hydro-Québec, Varennes, Québec, Canada

E-mail: Andre.Kukushkin@iter.org

**Abstract**. The paper describes the results of a physics analysis of a modified divertor cassette for ITER. The issues addressed are the impact on the operational window, the effect of gas leaks through the broader gaps between the divertor cassettes, and radiation power loading of different components of the cassettes. The radiation load on the side walls of the cassette structures in the inter-cassette gaps is identified as a design constraint not previously considered.

## 1. Introduction

This paper reports results of the current optimisation of the set of divertor cassettes to be installed in the initial phase of ITER. Studies performed during the course of the ITER Design Review had revealed that the original divertor geometry [1] imposed excessive requirements on the accuracy of the plasma position control system because it strongly constrained the allowable positions of the magnetic separatrix. The key elements of the new optimisation are lowering the divertor dome and reducing its size, Fig. 1. The inner target is moved outwards and tilted somewhat less with respect to the magnetic surfaces in order to accommodate a wider range of ITER plasma equilibria with flatter current profiles in the core ($l_i \geq 0.6$ vs. original 0.85, [2]). Furthermore, the reflector plates connected to the lower ends of the targets are rendered more horizontal in order to avoid direct plasma contact of their leading edges during possible excursions of the separatrix by placing them in the shadow of the reduced dome. On one hand, this modification reduces the power handling capability (in terms of parallel flux) as the attack angle of the magnetic field line at the target increases. On the other hand, it improves the ability of divertor infra-red diagnostics to see all the way down to the divertor corner and therefore of the separatrix position control.

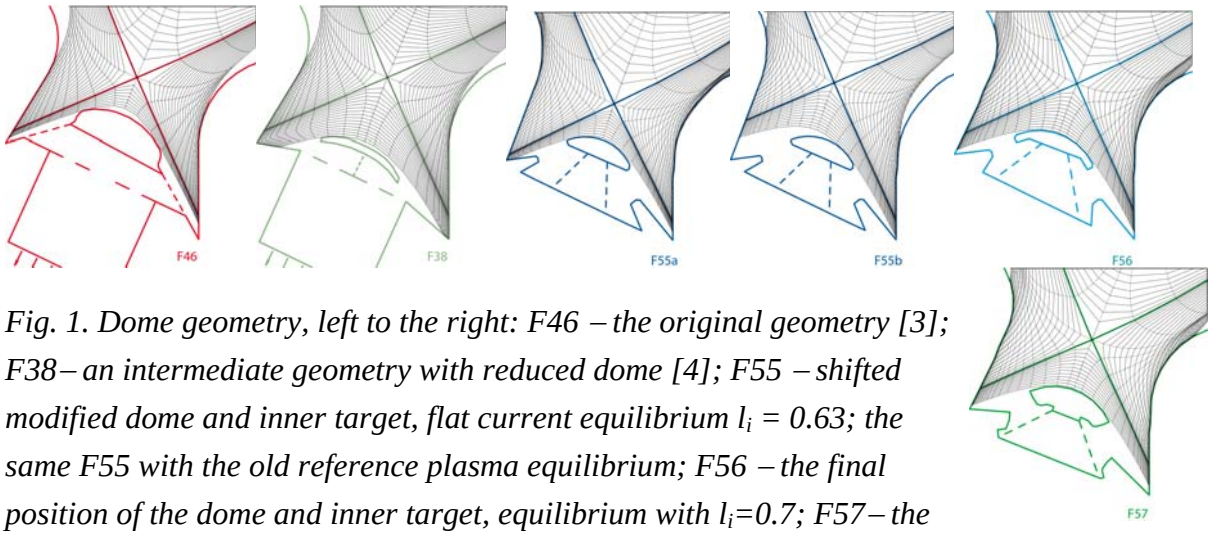


*Fig. 1. Dome geometry, left to the right: F46 – the original geometry [3]; F38 – an intermediate geometry with reduced dome [4]; F55 – shifted modified dome and inner target, flat current equilibrium $l_i$ = 0.63; the same F55 with the old reference plasma equilibrium; F56 – the final position of the dome and inner target, equilibrium with $l_i$=0.7; F57 – the reflector plates in the final position. Dashed lines show partially transparent structures giving access to the pump ducts. (No calculation results available for F57 yet).*

To increase the flexibility for the equilibrium control system, the control philosophy is changed allowing transient X-point positions much lower than the reference equilibrium. Note that with the existing design specifications, the reflector plates can cope without major problems with the expected transients. The structures carrying the dome are now more robust, and the space below the dome is more open to the private-flux region (PFR) plasma. For technological reasons, the poloidal gaps between the divertor cassettes have been increased from 10 to 20 mm, exposing however the side surfaces of the cassettes to radiation from the plasma and increasing the gas circulation in the divertor.

Preliminary results of an analysis of the consequences of such modifications for the divertor performance, from both physics and engineering points of view were reported in [5] - the analysis is continued here. Because divertor modelling is very time-consuming, the study necessarily involves examination of divertor variants already considered earlier to anticipate the expected parameter variation. Below we examine the effect of the modification of the divertor shape on the edge plasma performance (Sec. 2), the enhanced gas circulation through the inter-cassette gaps (Sec. 3), and the surface and gap radiation load (Sec. 4).

## 2. Effect of Divertor Modification on the Edge Plasma Performance

The B2-Eirene code package, version SOLPS4.3 [5] is used for the edge modelling described here. The code employs a two-dimensional fluid description for the ions and electrons of the edge plasma, and a full three-dimensional kinetic Monte-Carlo simulation for the neutrals, taking into account neutral-neutral and molecule-ion collisions. In this study, the plasma consists of D (representing both D and T isotopes) ions, atoms, and molecules, as well as of He and C ions and atoms. Since the emphasis is on the effect of the divertor geometry modification, only carbon targets were selected for the first study – the data base of existing runs is largest for this option.

The effects of the dome modifications are shown in Fig. 2 where different parameters characterizing the divertor performance are plotted against the normalised neutral pressure in the divertor, $\mu$ ([6]; full inner divertor detachment is at $\mu = 1$). For the flat-current case, detachment of the inner divertor is found to occur at a 30%, and for the F56 geometry at a 50%, lower neutral pressure. When the normalization of $\mu$ is adjusted correspondingly for those cases, the detachment state of all cases is the same, and the peak temperature at the inner divertor superposes (Fig. 2a). As shown in Fig. 2b, the peak power loading for the old reference equilibrium with $l_i = 0.85$ (solid lines) decreases progressively as the dome size decreases from F46 through F38 to F55. (For the latter case, the power load, usually maximum on the outer divertor, actually peaks on the inner divertor.) Since the divertor operation window is limited by full detachment of either divertor ($\mu \leq 1$), this reduction of $q_{pk}$ expands the operational window towards lower neutral pressure – or lower edge density, thus increasing the operational flexibility of the divertor for the old reference equilibrium. For the plasma equilibrium consistent with flatter current profiles, the divertor asymmetry increases for the modified geometries F55 and F56, and the resulting peak power load (dashed lines in Fig. 2b) is then the same as for the old reference equilibrium in the original geometry F46. With respect to the power loading, the effect of the proposed modification on the operational flexibility of the ITER divertor is therefore either positive or neutral.

As concerns the effect on the core plasma fuelling, the DT ion density at the separatrix remains low (although up to 50% higher than for the original divertor, Fig. 2c), so that a strong density gradient in the pedestal region is still required to provide the necessary plasma density in the core ($\sim 10^{20}$ m$^{-3}$). The variation of the neutral particle influx across the separatrix (Fig. 2d) is minor and the influx remains small in magnitude, $\leq 20$ Pa-m$^3$/s. Since

this is insufficient to fuel the core (which may require ~ 100 Pa-m$^3$/s [7]), the need for extra core fuelling is unchanged with the modified divertor.

The conditions for helium removal become worse by a factor 2-3 for the modified divertor (higher separatrix density, Fig. 2e, and same neutral influx, Fig. 2f, for the old reference equilibrium F55, higher influx and the same density for the low-$l_i$ case and F56). Nevertheless, this is a smaller deterioration than for the complete dome removal discussed in [4], and the levels remain low (edge density <$10^{18}$ m$^{-3}$, neutral reflux < 1 Pa-m$^3$/s), so that, as demonstrated by integrated modelling of the core plasma performance in ITER [7, 8], the resulting helium level in the core is low and therefore this increase of the helium does not modify the ITER operating window significantly.

On the whole, the proposed divertor modification fits the qualitative picture developed in [4]: a reduction of the dome renders the divertor more in-out symmetric, which is beneficial for the peak power loading on the targets but somewhat detrimental for helium removal. Moreover, the new divertor offers some degree of detachment asymmetry control by changing the position of the separatrix strike point at the inner target.

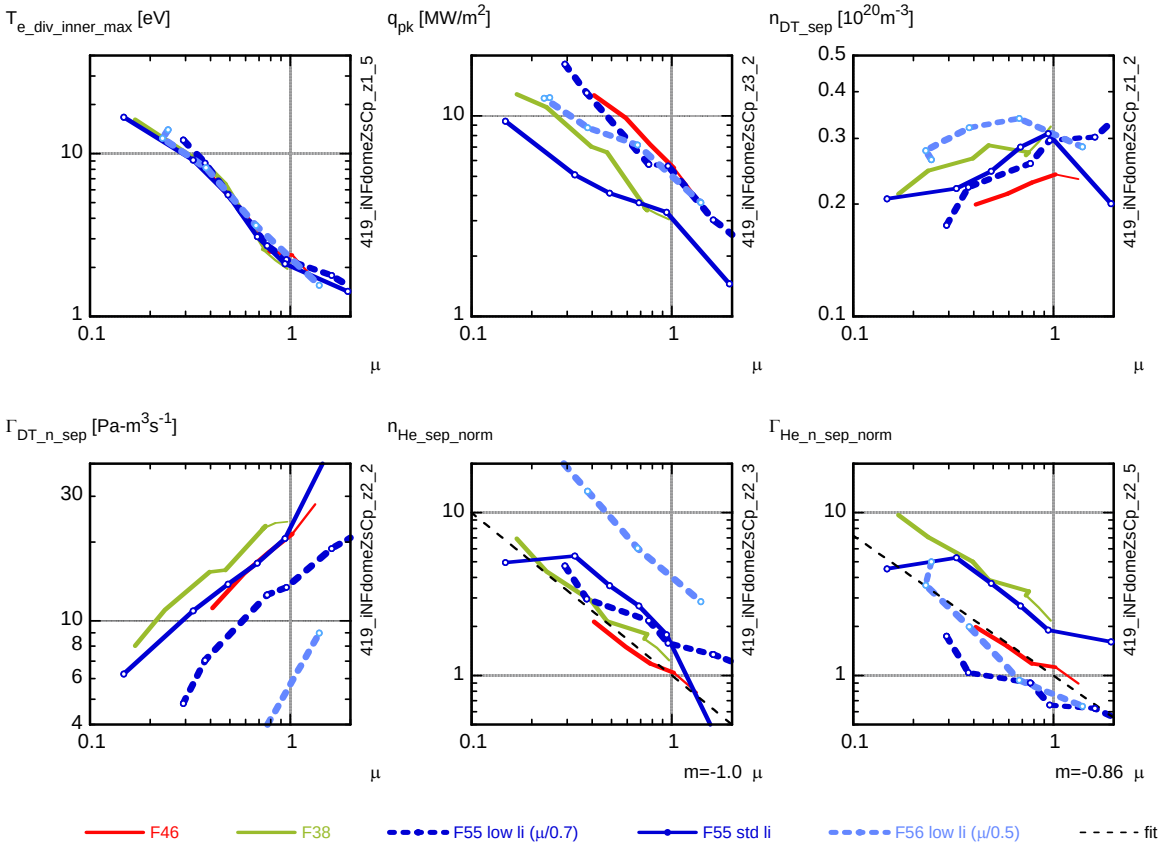


*Fig. 2. Modelling results vs. normalized neutral pressure under the dome, μ [3], for the divertor geometries considered: (a) maximum temperature at the inner divertor target (b) peak power loading of the targets; (c) average fuel ion density at the separatrix;(d) fuel neutral influx to the core; (e) average helium ion density at the separatrix; (f) helium neutral influx to the core. The helium data are normalized to the helium production rate and pumping speed [6]. Solid lines refer to the old reference equilibrium; dashed lines to low-$l_i$ (see text).*

## 3. Effect of the Inter-Cassette Gaps on Divertor Performance

In order to permit replacement of the divertor components in reasonable time, a modular design is employed for the ITER divertor. The latter consists of 54 cassettes positioned

symmetrically in the toroidal direction [1], which can be installed or removed remotely. Unavoidably, gas leaks will be present associated with the poloidal gaps between the cassettes. In the current revised design these gaps are made wider, 20 mm, in order to ensure the uniformity of the cassette modules and to facilitate the remote handling. The inter-cassette gaps will change the gas flow pattern inside the divertor, which might affect both the plasma performance and the pumping conditions. (The effect on radiation loads is treated in the next section.)

The first study of the effect of the inter-cassette gaps was reported in [9] for the previous reference design with narrow gaps 5 to 10 mm wide. No major deterioration of the divertor performance in terms of either power loading or core fuelling or helium removal was found, and therefore, because the target components are also thicker in the current design and the gas conductance of a gap is inversely proportional to its depth, a further increase of the gap width to 20 mm is expected to result in an equally minor effect. There was however one caveat in the consideration of [9], namely, the targets were assumed to be perfectly sealed and saturated. Code runs with a full cassette model including the realistic cassette geometry with all the gaps taken into account will be done in future. For now, a rough estimate of the effect of the gaps in the target area can be extracted from a limited series of runs for which a partial absorption of incident ions and atoms at the target was assumed, compensated by a uniform gas outflow per unit area from the whole target surface and equal for both inner and outer divertors. The recycling is therefore made non-local, and this is expected to be the major effect of the presence of the gaps.

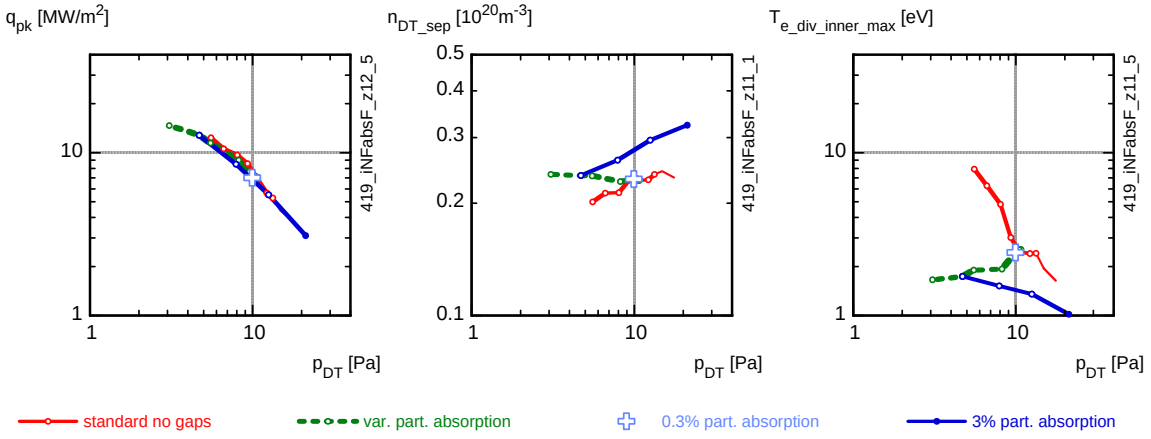


*Fig. 3. Effect of non-local recycling at the targets. The peak power on the targets, the fuel density upstream, and the maximum electron temperature at the inner target are shown vs. neutral pressure in PFR for the standard assumption of fully saturated target surface and 3% particle absorption compensated by a uniform outflux. The divertor geometry corresponds to the previous reference design [3].*

The results of this study are shown in Fig. 3 where the variation of $q_{pk}$, $n_{DT\_sep}$, and $T_{e\_max}$ in the inner divertor along with the neutral pressure in PFR, $p_{DT}$, is compared for the cases of fully saturated target surface (local recycling) and with 0.3% and 3% of the particle flux absorbed and an equal amount re-emitted uniformly from the targets. The 3% absorption level corresponds to the geometric ratio of the gap to the cassette width without taking account of the gap conductance. Since in a long tube (narrow gap) the gas conductance is ~ $d/L$, the gap conductance would actually modify the effective particle absorption by a factor ~ 0.1, i.e. the realistic situation would be expected to be closer to 0.3% than to 3% absorption in this model, and the poloidal distribution of the re-injected flux will not be uniform.

For this over-estimated particle recirculation on the targets at the 3% level, the plasma parameters at the outer targets – in particular, $q_{pk}$ – remain the same, the conditions for helium removal do not change, but the inner divertor would become more detached, Fig. 3c, and the operational window would therefore be reduced. However, the more realistic value of 0.3% effective absorption does not appear to produce a strong effect at least for the single data point available so far. Studies taking account of the gap conductance which will reduce the effective absorption and modify the poloidal distribution of the re-injected flux are required and will be done in the near future to improve evaluation of the effect of the enhanced inter-cassette gaps on the divertor performance in ITER.

## 4. Radiation loads

The ITER operational regimes with partial detachment of plasma from the targets rely on strong radiation from the edge. For the operational window shown in Fig. 2, the fraction of the power transferred to the SOL and divertor that is radiated is 60 to 80%, and most of this radiation occurs in the divertor. Whereas these loads are included in the calculated power loading of the high heat flux components such as divertor targets and baffles, the radiation loads on structural elements of the divertor cassette require special evaluation, since the heat removal capacity of these elements is significantly lower than that of the high heat flux components. The frontal radiation load on different cassette components was calculated from three B2-Eirene runs using the F56 geometry, corresponding to the low, medium, and high density points from Fig. 2. The results are shown in Fig. 4, plotted along the contour also shown there.

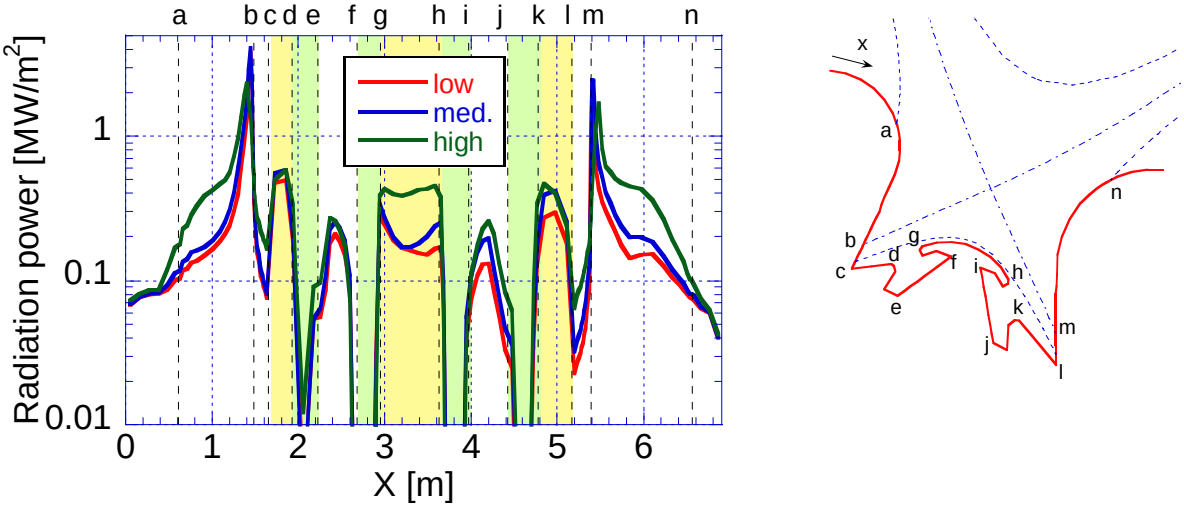


*Fig. 4. Left: radiation power loads on the structures in PFR for the modified dome F56 for three operational points: at low density, intermediate, and near the high-density limit (full detachment) of the operational window. Right: Geometry layout for the evaluation of the radiation. The loads are given along the contour marked red, with x=0 at the inner baffle. The separatrix and the limits of the computational grid are also shown.*

Other than the radiation loads on the front surfaces of the cassette structures which are already an integral part of the design requirement, those on the lateral surfaces via the inter-cassette gaps can also be important for the cooling design. In order to estimate this effect from our 2D modelling results, consider a simplified geometry. Suppose that all the radiation entering the gap from the plasma originates from a toroidal linear radiation source, and assume the

cylindrical approximation ($R >> a$), Fig. 5. The unit intensity of the radiation from the linear source is $dI = 1/\left(4\pi r^2\right) I_0 dx$ where $I_0$ is found from the known radiation load on the gap entrance surface $q_{rad}$, equal to the target load calculated by the 2D model, i.e. $I_0 = 2\pi b q_{rad}$ .

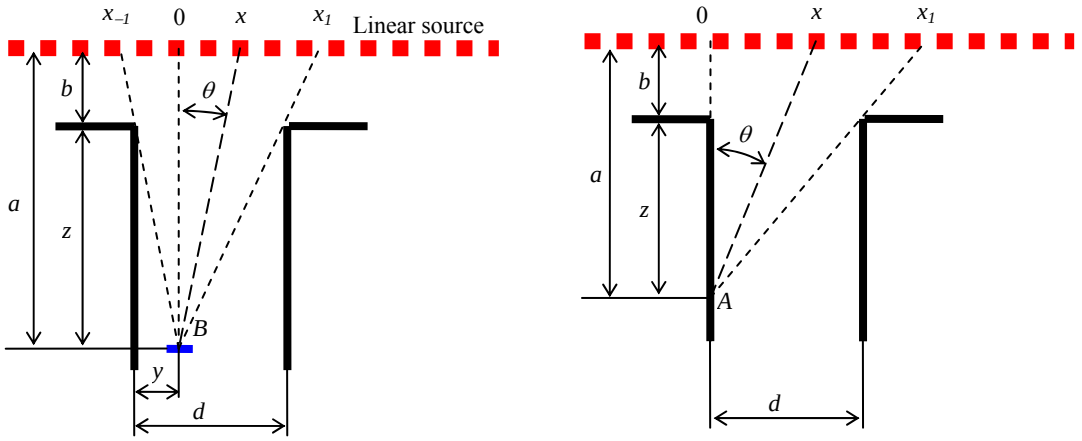


*Fig. 5. Geometry schematics for the estimation of radiation loads in a poloidal gap with fully absorbing walls: bottom (left) and side wall (right). The linear radiation source is oriented toroidally (x co-ordinate).*

Suppose that the gap walls are perfectly absorbing (no reflection), and consider first the load on a surface perpendicular to the gap, at the point *B*. It is irradiated from the segment ($x_{-1}$,$x_1$) of the source, where $x_{-1} = -y\,{}^{a}\!/_{z}$, $x_1 = (d-y)\,{}^{a}\!/_{z}$. The radiation flux at the point *B* is then

$$q_b(z,y) = \int dI \cos\theta = \frac{aI_0}{4\pi}\int_{x_{-1}}^{x_1} \frac{dx}{\left(a^2+x^2\right)^{3/2}} = q_{rad}\,\frac{b}{2a}\,\frac{x}{\left(a^2+x^2\right)^{1/2}}\Bigg|_{x_{-1}}^{x_1} \qquad (1)$$

(note $a = z + b$). In the limit of large $z$, $z >> \max(d,b)$, Eq. (4) yields $q_b \cong {}^{1}\!/_{2}\,{}^{b}\!/_{z}\,{}^{d}\!/_{z}\,q_{rad} \propto z^{-2}$.

Now consider the radiation loads on the gap walls. Since the problem is toroidally symmetric, it is sufficient to consider one side of the gap, Fig. 5b. The radiation flux onto the gap wall at the point A is then

$$q_a(z) = \int dI \sin\theta = \frac{I_0}{4\pi}\int_0^{x_1} \frac{x\,dx}{\left(a^2+x^2\right)^{3/2}} = -q_{rad}\,\frac{b}{2a}\,x^{-1/2}\Bigg|_1^{1+{}^{d^2}\!/_{z^2}}, \qquad (2)$$

Near the gap entrance, $z = 0$, Eq. (5) yields $q_a = 0.5 q_{rad}$, and deep in the gap where $z >> \max(d,b)$, $q_a \cong {}^{1}\!/_{4}\,{}^{b}\!/_{z}\left({}^{d}\!/_{z}\right)^2 q_{rad} \propto z^{-3}$.

These estimates can be generalized to take into account an imperfect specular reflection at the side walls with the reflection coefficient $R_s$. (The specular reflection is selected here for simplicity – the real reflection is not specular.) Simple geometrical considerations taking into account the symmetry of the problem as shown schematically in Fig. 6, give:

$$q_a^R(z,R_s)=\frac{I_0}{4\pi}\sum_{k=0}^{\infty}R_s^k\int_{x_k}^{x_{k+1}}\frac{xdx}{\left(a^2+x^2\right)^{3/2}}=-q_{rad}\frac{b}{2a}\sum_{k=0}^{\infty}R_s^k x^{-1/2}\Bigg|_{1+k^2d^2/z^2}^{1+(k+1)^2d^2/z^2} \tag{3}$$

for the radiation power flux on the gap walls, and

$$q_b^R(z,y)=\frac{I_0}{4\pi}\sum_{k=-\infty}^{\infty}R_s^{|k|}\int_{x_k}^{x_{k+1}}\frac{dx}{\left(a^2+x^2\right)^{3/2}}=q_{rad}\frac{b}{2a}\sum_{k=-\infty}^{\infty}R_s^{|k|}\frac{x}{\left(a^2+x^2\right)^{1/2}}\Bigg|_{x_k}^{x_{k+1}}, \tag{4}$$

for the radiation flux at the point *B*. Here $x_m=(md-y)a/z$.

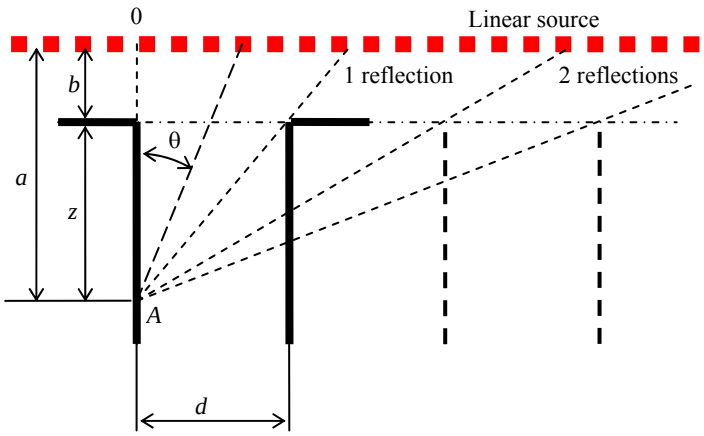


*Fig. 6. Geometry schematics for the estimation of side wall radiation loads in a poloidal gap with finite specular reflection.*

Note that Eq. (7, 8) give the incident power flux on the surface. In order to obtain the absorbed power transferred to the material there, these values should be multiplied by $(1-R_m)$, where $R_m$ is the reflection coefficient of the material there. The profiles of $q_a^R, q_b^R$ for different values of parameters $b$ and $R_s$ are shown in Fig. 7. Variation of the $b$ value can be used to estimate the effect of the poloidal width of the $q_{rad}$ profile (perpendicular to the plane of Fig. 5 and 6), at least for the peak value of the power: $b$ = 5000 mm would correspond to a uniform profile whereas a linear source with $b$ = 100 mm would produce a 0.2 m wide radiation profile on the target. One can see that the peaked profiles of $q_{rad}$ lead to a faster decay of the radiation power flux in the gap.

The values of $q_a^R, q_b^R$ as given by Eq. (3, 4) can be used to estimate the radiation power loading on the sides of the gaps between the divertor cassettes or on diagnostic equipment placed in these gaps. The gap width is $d$ = 20 mm, and the parameter $b$ can be selected to emulate the poloidal profiles of $q_{rad}$ estimated from B2-Eirene calculations (Fig. 2). For example, the maximum radiation power is about 4 MW/m$^2$ on the inner target, and the profile width there about 200 mm hence $b$ = 100 mm should be used for the estimate. The steel body of the target starts about 50 mm below the plasma-facing surface (PFS), hence the radiation power there, assuming $R_s=R_m=0.5$, is about a factor 6 lower, Fig. 5a, than near the gap entrance where it is $(1-R_m)\,q_a^R(0)\cong 1$ MW/m$^2$. The power deposited on the steel surface is

then ~ 0.15 MW/m$^2$ and lower by an order of magnitude to the back end of the gap (150 mm from the PFS), and this should be taken into account for the cooling design.

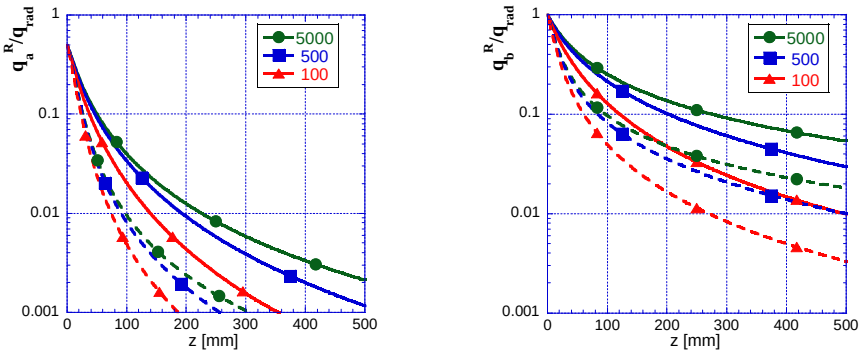


*Fig. 7. Profiles of incident radiation load in the inter-cassette gaps with specular reflection $R_s$ for different values of parameter b (given in the legend in mm) and different values of reflectivity $R_s$ (solid 0.5, dashed 0): $q_a^R(z)$ (left) and $q_b^R(z)$ (right). The z co-ordinate is directed perpendicular to the PFS down the gap. The gap width d = 20 mm.*

## 6. Conclusions

The modified geometry of the divertor which is now included in the baseline ITER design offers more flexibility for the magnetic configuration, reducing the requirements to the control system and increasing the reliability of the machine operation. The resultant modification of the divertor performance and its operational space has been analysed and shown to have a beneficial or neutral impact. An initial estimate of the effect of wider gaps between the cassettes indicates only minor effects on divertor performance, but it needs to be refined in future. Data on power loading of different divertor components have been obtained and will be used as the basis for the refined cassette design, and the radiation delivered to the side walls of the cassette elements by radiation through the inter-cassette gaps is identified as a design constraint not previously considered.



[1] R. Tivey, E. D'Agata, V. Chuyanov, H. Heidl, Fusion Eng. Design **75–79** (2005) 447.
[2] C. E. Kessel, G. Saibene, Y. Gribov, et al., this conference, paper IT/2-3.
[3] A.S. Kukushkin, H.D. Pacher, G.W. Pacher, *et al.*, *Nucl. Fusion* **43** (2003) 716.
[4] A.S. Kukushkin, H.D. Pacher, V. Kotov, et al., Proc. 34th Eur. Conf. on Contr. Fusion and Plasma Phys., Warsaw 2007, paper P1-061.
[5] A.S. Kukushkin, H.D. Pacher, V. Kotov, *et al.*, Proc. 35th Eur. Conf. on Contr. Fusion and Plasma Phys., Hersonissos 2008, paper P1.013.
[6] H.D. Pacher, A.S. Kukushkin, G.W. Pacher, *et al.*, 18th PSI Conference, Toledo, May 2008, paper O-27 (to appear in *J. Nucl. Mater.*).
[7] G.W. Pacher, H.D. Pacher, G. Janeschitz, A.S. Kukushkin, *Nucl. Fusion* **48** (2008) 105003.
[8] G.W. Pacher, H.D. Pacher, A.S. Kukushkin, G. Janeschitz, Proc. 35th Eur. Conf. on Contr. Fusion and Plasma Phys., Hersonissos 2008, paper P4.079.
[9] A.S. Kukushkin, H.D. Pacher, V. Kotov, et al., *Nucl. Fusion* **47** (2007) 698.